Polymer Degradation and Stability 234 (2025) 111204

Contents lists available at ScienceDirect

Polymer Degradation and Stability

journal homepage: www.journals.elsevier.com/polymer-degradation-and-stability

Photochemical degradation of PLA-based green composites containing waste biomass from *Posidonia oceanica, Chamaerops humilis* and *Ailanthus altissima*: A comparative study

Andrea Maio, Emmanuel F. Gulino, Michele Gammino, Maria Clara Citarrella, Roberto Scaffaro *

Department of Engineering, University of Palermo, Viale delle Scienze, Palermo, Italy

ARTICLE INFO

Keywords:
Degradation
Green composites
Photo-oxidation
Accelerated weathering
UV

ABSTRACT

The photochemical degradability of PLA-based composites containing three different natural fillers, namely *Posidonia oceanica* (PO), *Chamaerops humilis* (CH), and *Ailanthus altissima* (AA), was evaluated to understand how the morphological and physicochemical features of these composite systems affect their durability. Composites containing 10% or 20% of filler were prepared by melt-processing and subjected to accelerated weathering involving UV irradiation and condensation cycles. The materials were thoroughly characterized, and the evolution of morphological, physicochemical, and mechanical properties was monitored upon aging time. The results demonstrate the significant impact of filler type on the photochemical stability of PLA-based composites. PO and CH fillers, with high porosity, resulted in less compact composites that underwent rapid hydrolytic degradation, experiencing surface and bulk erosion. AA composites exhibited the highest durability, with their dense morphology effectively delaying degradation. Overall, composites with 10% PO and 20% CH had the lowest stability (less than 6 h), the other PO- and CH-series materials retained durability for 24–30 h, similar to neat PLA, while AA-series composites proved to retain their mechanical properties for up to 36 h.

1. Introduction

The pressing concern about environmental issues and global pollution garnered the attention of scientific community towards bioplastic and related "green" composites [1–3]. Among the biodegradable polymers, polylactic acid (PLA) offers one of the most promising alternatives to traditional plastics, especially in applications where environmental impact and biodegradability are critical [4,5]. Moreover, replacing portions of expensive PLA with cost-effective waste biomass brings additional benefits, including high tensile strength and stiffness, but also presents challenges related to thermal stability, brittleness, and durability.

Biodegradable polyesters, such as poly(lactic acid) (PLA), are susceptible to various degradation mechanisms during processing, usage, and disposal. The presence of green fillers from waste biomass can either accelerate or delay these processes, depending on several factors. While rapid degradation during disposal is desirable, minimizing degradation during processing and service life is strategic to optimize their performance from both economic and environmental perspectives [6,7]. In fact, green composites with adequate UV ageing resistance could be highly suitable for outdoor applications, such as eco-friendly garden furniture, flowerpots, and other decorative items, as well as rigid packaging solutions, including fruit and vegetable crates for outdoor markets. Furthermore, recent advances show the potential of green composites even in cutting-edge applications, such as water and air remediation, highlighting the importance of studying their durability in real-world conditions [8,9].

Specifically, PLA undergoes hydrolytic degradation when exposed to moisture over time, a process accelerated at high temperatures, such as during melt processing [10]. The presence of rigid, hydrophilic fillers like lignocellulosic ones may exacerbate thermomechanical and hydrolytic degradation during processing and after disposal. Conversely, lignin domains in natural fillers can provide UV-shielding, protecting the polymer matrix from photochemical aging and thereby enhancing the service life of the products [8,11,12].

A deep understanding of the degradability of bioplastic-based green

* Corresponding author.
E-mail address: roberto.scaffaro@unipa.it (R. Scaffaro).

https://doi.org/10.1016/j.polymdegradstab.2025.111204
Received 28 October 2024; Received in revised form 11 December 2024; Accepted 17 January 2025
Available online 18 January 2025

composites in different scenarios is crucial for properly assessing their environmental performance. This knowledge can facilitate the fabrication of green composites that combine adequate performance during their service life with relatively fast disintegration after disposal [13].

In our previous research, our group studied the disintegrability of PLA-based biocomposites containing *Posidonia Oceanica* (PO) flour when stored in neutral and alkaline aqueous solutions, finding that biocomposites degraded much faster than neat polymer [14]. Specifically, we evidenced the crucial role of PO, capable of both imparting degradation to PLA during processing with enhancement of hydrophilicity and offering preferential gateways for solution penetration through filler-matrix interface by capillarity and swelling-aided polymer cracking. On the other hand, recent studies reported that some lignocellulosic fillers obtained from rice husk, hazelnut shell, as well as wood flour, can serve as photo-stabilizers for PLA, because lignin domains act as a UV-shield [15,16]. Therefore, it could be inferred that fillers containing large amount of lignin but especially those containing flavonoids, polyphenols and various types of antioxidant compounds may somehow protect the host polymers from degradation. Indeed, in another study, our group demonstrated that lignocellulosic fibers coming from dwarf palm Chamaerops humilis (CH) had a fair effect on the stabilization of PLA during melt processing, providing a good retention of polymer molar mass, especially when compared to pro-degradant PO fillers, while having a scarce tendency to give rise to dense materials [17]. Indeed, porosity of hydrolysable materials, such as green composites, is a critical factor that affects UV and solution penetration and the surface area exposed to chemical and photochemical degradation reactions. [18–22]. Lignocellulosic fillers possess unique characteristics that are vital for enhancing the degradability of bioplastics, particularly their hydrophilicity and intrinsic porosity resulting from the presence of lumens. [23,24]. Green composites containing lignocellulosic fillers, such as *Posidonia oceanica, Chamaerops humilis*, and *Ailanthus altissima*, should be considered porous materials, as the polymer macromolecules can partially fill the voids within these particles [25–27]. However, the varying pore architecture and porosity of lignocellulosic fillers, combined with the characteristics of the polymer and the processing conditions, can result in materials with different levels of porosity. This property significantly influences the mechanical properties of all green composites and may also be crucial for their durability [25,28].

Recently, many studies highlighted the huge potential of *Ailanthus altissima* (AA) as a source for antioxidant compounds [29–32]. In particular, the mechanisms involved are both the prevention and the scavenging of radical oxygen species [32,33]. *Ailanthus altissima* swingle (Simaroubaceae), also known as the tree of heaven, is an alien weed plant, considered dangerous for ecosystems and biodiversity, although being characterized by vast pharmacological potential because of its rich phytochemical profile [32]. Surprisingly, to the best of our knowledge, no study was reported so far on the possibility to use fibers extracted from this plant as potential reinforcement for polymer-based composites.

The aim of this work is to evaluate the photochemical degradability of PLA-based composites containing three different natural fillers, namely *Posidonia oceanica* (PO), *Chamaerops humilis* (CH), *Ailanthus altissima* (AA), to understand the effect of morphological and physicochemical features of such composite systems on their durability.

2. Experimental part

2.1. Materials and methods

The polymer selected as a matrix was an extrusion grade sample of polylactic acid (PLA), namely Ingeo 2003 D (NatureWorks), having a content of D-lactic acid monomer equal to ~ 4%, density (ρ) = 1.24 g/cm^3, melt flow index (MFI) = 6 g/10 min, melting temperature (T_m) = 160 °C, and Mw = 240 kDa. The lignocellulosic fillers selected were flours obtained from waste *Posidonia oceanica* (PO), *Chamaerops humilis* (dwarf palm) (CH), and *Ailanthus altissima* (AA). PO and CH waste were collected from the western sea-cost of Palermo (coordinates: 38°06′56″N13°21′41″E), while AA waste was sourced from the university campus park of the University of Palermo (coordinates: 38°05′15.6″ N 13°20′57.8″E) where the plant was being removed as part of invasive species management efforts. The lignocellulosic waste was rinsed with water, dried, and ground using a ball mill (MM 500 Nano, Retsch) under the following conditions: 10 Hz, 15 min, with a 20 mm-diameter ball. The resulting flour was then sieved, and the fraction below 100 μm (140 mesh) was collected and used as filler. Chloroform (reagent grade) was purchased from Sigma Aldrich.

2.2. Preparation and characterizations

Green composites containing 10 wt.% or 20 wt.% of PO, CH or AA were prepared by melt mixing in an internal batch mixer (Brabender Plasticorder). For each batch, filler and matrix – previously dried in a vacuum-oven overnight at $T = 90$ °C to avoid hydrolytic reactions during processing – were premixed at the solid state and fed into the batch mixer. The compounding was conducted at the following operating conditions: T = 190 °C, rotor speed = 64 rpm, t = 6 min, which were optimized based on our previous works [14,25,28]. The material, collected after melt processing, was rapidly cooled by liquid nitrogen, ground into pellets and compression-molded (Carver laboratory press) at 190 °C and 8 bars for 90 s and finally cut into rectangular specimens (length=90 cm, width=10 cm, thickness=300 μm) for the further characterizations.

Photochemical aging of the samples was performed in a Q-UV Solar Eye weatherometer equipped with UV-B lamps (313 nm), with cycles comprising 4 h of irradiation at $T = 55$ °C followed by 2 h of dark/condensation at $T = 35$ °C.

Gravimetric measurements were conducted to gain information about the evolution of mass during aging time: the residual mass degree (M_r) and its complement to 1 (i.e., Mass loss degree) were easily calculated by Eqns (1)-2, respectively, whereas the water uptake (%) was assessed by Eq. (3):

$$M_r = \frac{M_{t,dry}}{M_0} \tag{1}$$

$$M_{loss} = 1 - M_r \tag{2}$$

$$Solution\ uptake\ (\%) = \frac{M_{t,wet} - M_{t,\ dry}}{M_{t,dry}} * 100 \tag{3}$$

Where M_0 is the initial weight of each specimen, $M_{t,wet}$ and $M_{t,dry}$ are respectively the specimen weight before and after drying. In fact, the aging protocol followed involves the contact of the samples with a liquid phase, i.e. water, during the condensation step. Therefore, photochemically aged samples, withdrawn at a given sampling time, were vacuum dried in oven at 90 °C for 10 h, prior to characterization.

Scanning Electron Microscopy (SEM) analysis was performed by an ESEM FEI QUANTA 200 onto both UV-exposed surface and cross-section of samples to monitor the time-evolution of morphology.

Photochemical transformations of the materials were investigated by Fourier-transform infrared (FTIR) spectroscopy in attenuated total reflection (ATR) mode, using a FT-IR/NIR Spectrum 400 spectrophotometer (Perkin-Elmer, Waltham, MA, USA). Spectra were collected in the 4000–450 cm^{-1} wavenumber range, by using 16 scans accumulations with a 4 cm^{-1} resolution. To allow an easier comparison between the materials treated at different photochemical aging times, spectra were normalized to the intensity of the CH_3 band at 1452 cm^{-1} after baseline correction, according to a reported protocol [15]. Areas under the spectral regions of interest (3800–3000 cm^{-1}, 1700–1490 cm^{-1}, 1800–1700 cm^{-1}) were determined to get further information about the photochemical reactions involved.

Surface wettability was assessed by measuring the water contact

Table 1
Salient characteristics of the three fillers used.

Sample	Skeletal density (g/cm^3)	Porosity after grinding (%)	Aspect ratio[a]	E_{bulk} (GPa)[b]
PO	1.54	70	6	~ 12
CH	1.51	51	15	~ 32
AA	1.50	34	12	~ 10

[a] calculated as D_{eq}/t for PO and AA (Eq. S1), and as L/D for CH.
[b] measured by tensile tests on raw fibers and calculated according to Eq. S2.

angle (WCA), in sessile drop mode using FTA1000 (First Ten Angstrom, UK) equipment. Specifically, a drop of water (2 μL) was dispensed from a micro-syringe onto the UV-exposed side of specimens with the image being acquired after 20 s.

Tensile mechanical properties, elastic modulus (E), tensile strength (TS) and elongation at break (EB), were determined by means of an Instron 3365 (Instron, USA) dynamometer, by imposing a crosshead speed of 1 mm/min up to specimen failure, according to ISO 527–3 standard. For each experimental run at least 7 replicates were tested. Toughness (k), herein intended as work-to-failure, was calculated via the integration of stress-strain curves. Data were provided as mean ± standard deviations.

Differential scanning calorimetry (DSC) was carried out by using a Shimadzu DSC-60 at a scanning rate equal to 10 °C/min within the temperature range 30–200 °C. The degree of crystallinity (χ) of PLA in each sample was calculated according to eqn. (4) [34]:

$$\chi = \frac{\Delta H_m - \Delta H_{cc}}{(1 - \Phi_w)\Delta H_m^0} \quad (4)$$

Where ΔH_m and ΔH_{cc} are, respectively, the melting enthalpy and the cold crystallization enthalpy, Φ_w is the filler weight fraction of the given composite, and ΔH_m^0 is the melting enthalpy of 100% crystalline PLA (93.7 J/g) [17,34].

To assess the molar mass of PLA, intrinsic viscosity measurements were carried out. For composites, the materials were dissolved in chloroform and repeatedly filtered to separate the filler phase from the polymeric phase. The polymer solutions were then exsiccated and re-dispersed in chloroform to prepare 0.13 wt% solutions, according to previous works [25,28].

Flow time was measured by means of iVisc LMV 830 Lauda Proline PV 15, Lauda-Königshofen, Germany) instrument equipped with a Ubbelohde (K = 0.009676) capillary viscometer, placed in thermostated oil bath at 30 °C. Intrinsic viscosity was then calculated using the Solomon-Ciuta equation, Eq. (5) [35]:

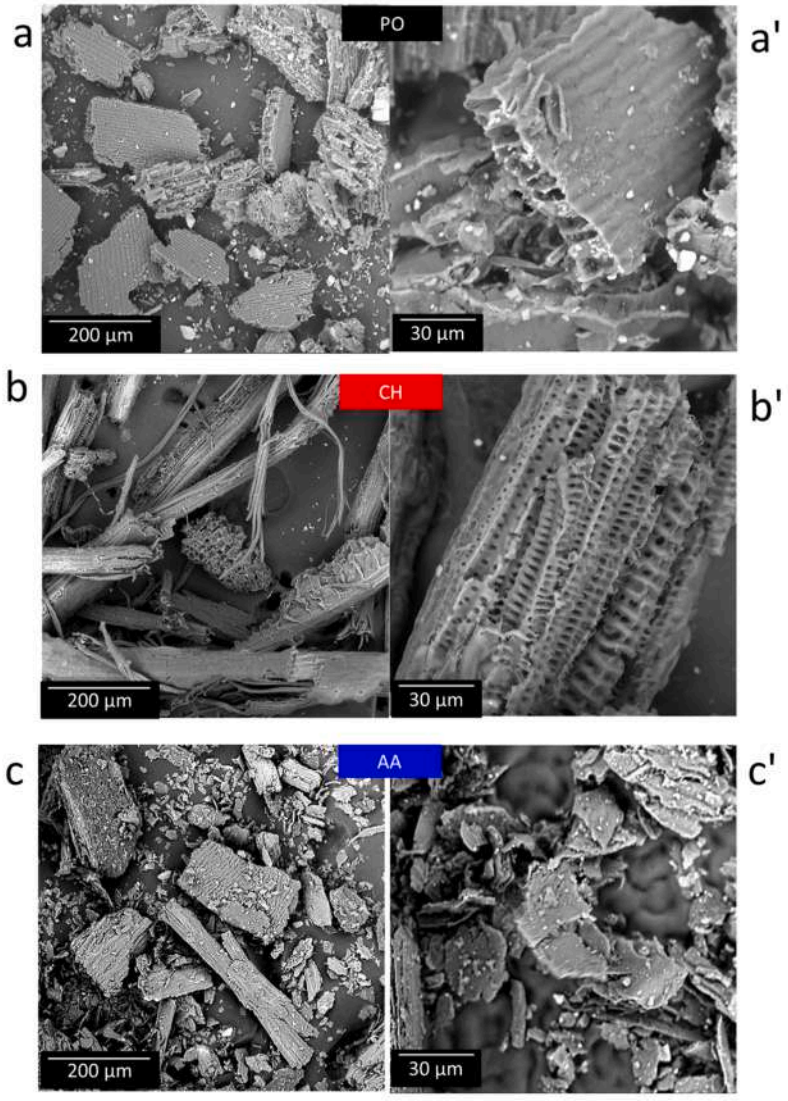

Fig. 1. SEM micrographs at different magnifications of PO powder (a-a'), CH powder (b-b') and AA powder (c-c') used as fillers for green composites.

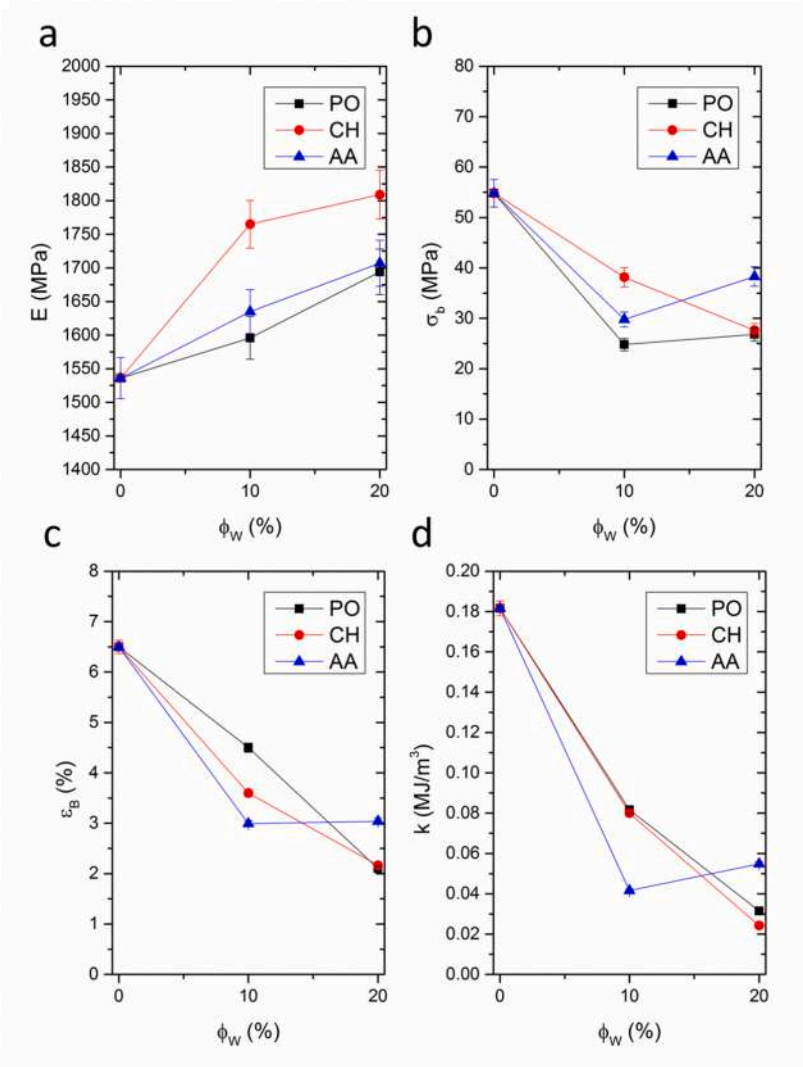

Fig. 2. Mechanical properties of the samples before aging: Elastic modulus (a), stress at break (b), elongation at break (c), toughness (d) plotted as a function of filler content.

$$[\eta] = \frac{\sqrt{2(\eta_s - \ln \eta_r)}}{C} \quad (5)$$

Where C is the concentration of the polymer solution, and η_s and η_r are the specific and the relative viscosities, respectively.

The viscosimetric molar mass (M_V) of PLA was extrapolated using Eq. (6):

$$M_V = \left(\frac{[\eta]}{K}\right)^{1/\alpha} \quad (6)$$

Where K and α are the Mark-Houwink constants of PLA/Chloroform system at 30 °C ($K = 0.0153$ mL/g and $\alpha = 0.759$ [26,36]).

The molar mass retention index was then calculated as the ratio between Mv of the given sample to that of unprocessed PLA (225,000 Da).

3. Results and discussion

The main characteristics of the three fillers used are reported in Table 1, whereas Fig. 1 provides the SEM micrographs of PO (a-a'), CH (b-b') and AA (c-c') at two different magnifications.

According to our previous findings, PO platelets can be approximated to highly porous parallelepipeds having constant thickness (25 μm) and variable length and width, with average values respectively equal to 160 μm and 75 μm, which result in an aspect ratio equal to 6. CH is a fibrous reinforcement with lower porosity and higher aspect ratio, which arises from lengths on the order of 2–5 mm s and diameters under a hundred micrometres [3,17,37,38].

Conversely, AA can be regarded as denser particles, heterogeneous in shape and dimensions, with a conspicuous number of thin platelets likely originated during ball milling (Fig. 1c'). As visible in SEM micrographs of Fig. 1, lateral size proved similar or slightly smaller than that of PO particles, but the thickness was lower (ranging from 2 to 10 μm), resulting in a higher aspect ratio.

It is acknowledged that starting characteristics of green composites are crucial for their durability when subjected to various types of degradation. For instance, the eventual effects of fillers on polymer degradation and/or crystallinity, as well as morphological parameters of multiphasic systems, including filler dispersion, interfacial adhesion, densification, are crucial to the overall performance of materials. Fig. 2a–d provides the main important mechanical properties, i.e., elastic modulus (E), tensile strength (TS), elongation at break (EB), and toughness (k), measured by tensile testing.

Basically, all the fillers display dose-dependent stiffening effects, with CH outperforming, while PO and AA based composites were found to show similar elastic moduli. The behavior of properties at break, instead, outlined a monotonic decrease with filler content for

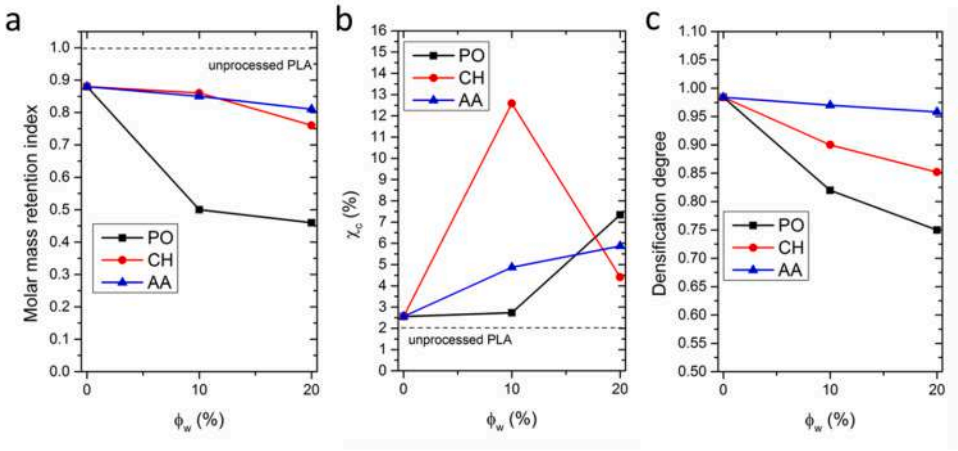

Fig. 3. Molar mass retention index, cristallinity and densification degree of materials before aging.

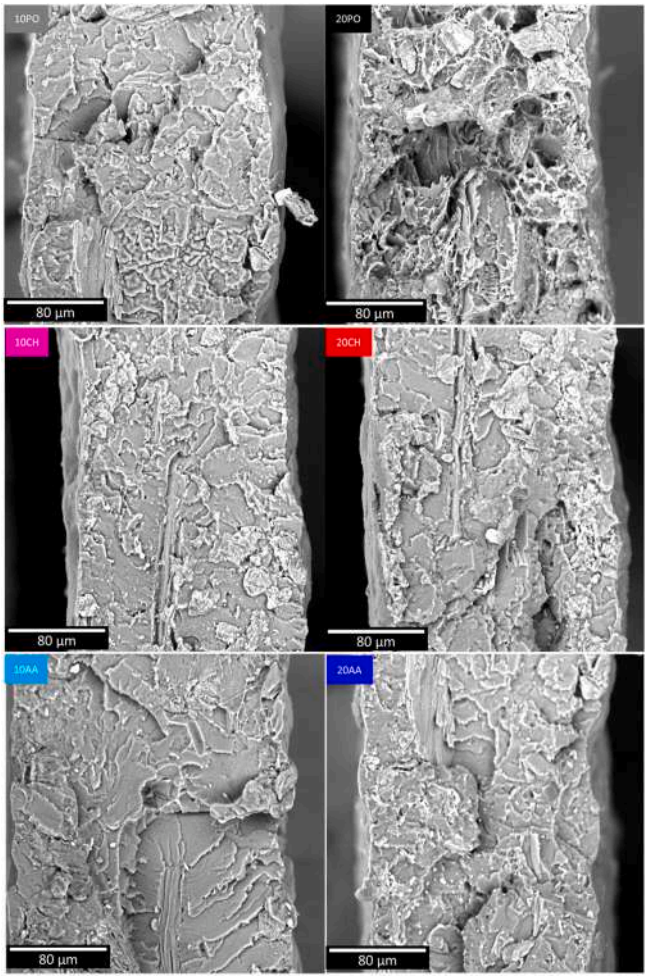

Fig. 4. Cross-sectional SEM micrographs of composites before aging.

composites containing PO and CH, as typically observed in the case of green composites, whereas AA-series materials at 20% had TS, EB, and toughness (k) slightly higher than those observed at 10%AA, although lower than those of neat matrix.

Fig. 3 provides a synoptic view of the initial state of green composites, outlined by monitoring the behaviour of some key-indicators, such as molar mass retention (Mv retention) and crystallinity of the polymer, densification, as a function of filler content and type.

Basically, AA-series composites displayed the highest degrees of M_v retention and densification, but low crystallinity. Notably, none of these properties proved to be influenced by filler content, except for a moderate increase in crystallinity. On the contrary, PO-series materials showed a dose-dependent monotonic decrease in PLA molar mass, likely due to pro-degradant activity of PO during melt processing and retained the amorphous nature of the matrix at 10%, while displaying significant increase in crystallinity at 20%PO. The densification degree of such composites was found to diminish upon increasing filler content, thus implying that most of PO lumina remain empty, as already reported.

CH-series composites displayed an intermediate performance in all these parameters, with the only exceptions of crystallinity degree, which was very sensitive to the filler content: CH10 displayed the highest result (12.6%), CH20 had only 4.40% crystalline region, likely because at the highest loading level, the filler hindered the ordering of macromolecules.

Aiming to assess the morphology of materials, in terms of filler dispersion, interfacial adhesion, SEM analysis was performed, and the cross-sectional micrographs of the samples are provided in Fig. 4.

All the samples display fair levels of filler dispersion and matrix-filler interfacial adhesion. However, the microstructure of AA-composites proved to be extremely more packed than that of CH-series and, especially, PO-series ones, in full agreement with the porosity values plotted in Fig. 3**c.**

Filler aspect ratio after processing, another important factor in composite systems, was discarded from this analysis, since all the fillers displayed significant breakage after melt mixing, with final values below 5 and the almost total disruption of their initial architecture. Both platelets and fibers proved to be transformed into heterogeneous microparticles with different size and geometry, as visible in Fig. S1.

The evolution of the elastic modulus (E), tensile strength (TS), elongation at break (EB), and toughness (k) during photochemical aging is shown in Fig. 5a–d, respectively. For each material, the properties were normalized to those of the unaged samples, and the time at which each property becomes half its initial value was esteemed (see the interception with the dotted lines at $y = 0.5$ in all graphs).

It is worth noting that semicrystalline polymers, such as PLA, may show an increase in elastic modulus and tensile strength due to crystallization phenomena occurring during aging. This can be attributed to chemi-crystallization resulting from the progressive shortening of polymer chains or structural rearrangement of macromolecules, as these materials are exposed to temperatures near their glass transition temperature (Tg). Elongation at break, typically considered a key indicator of aging in most polymers, may not be as significant here because PLA is glassy at room temperature and its initial EB value is low (refer to Fig. 2) [39,40]. Instead, a more suitable indicator of durability for such

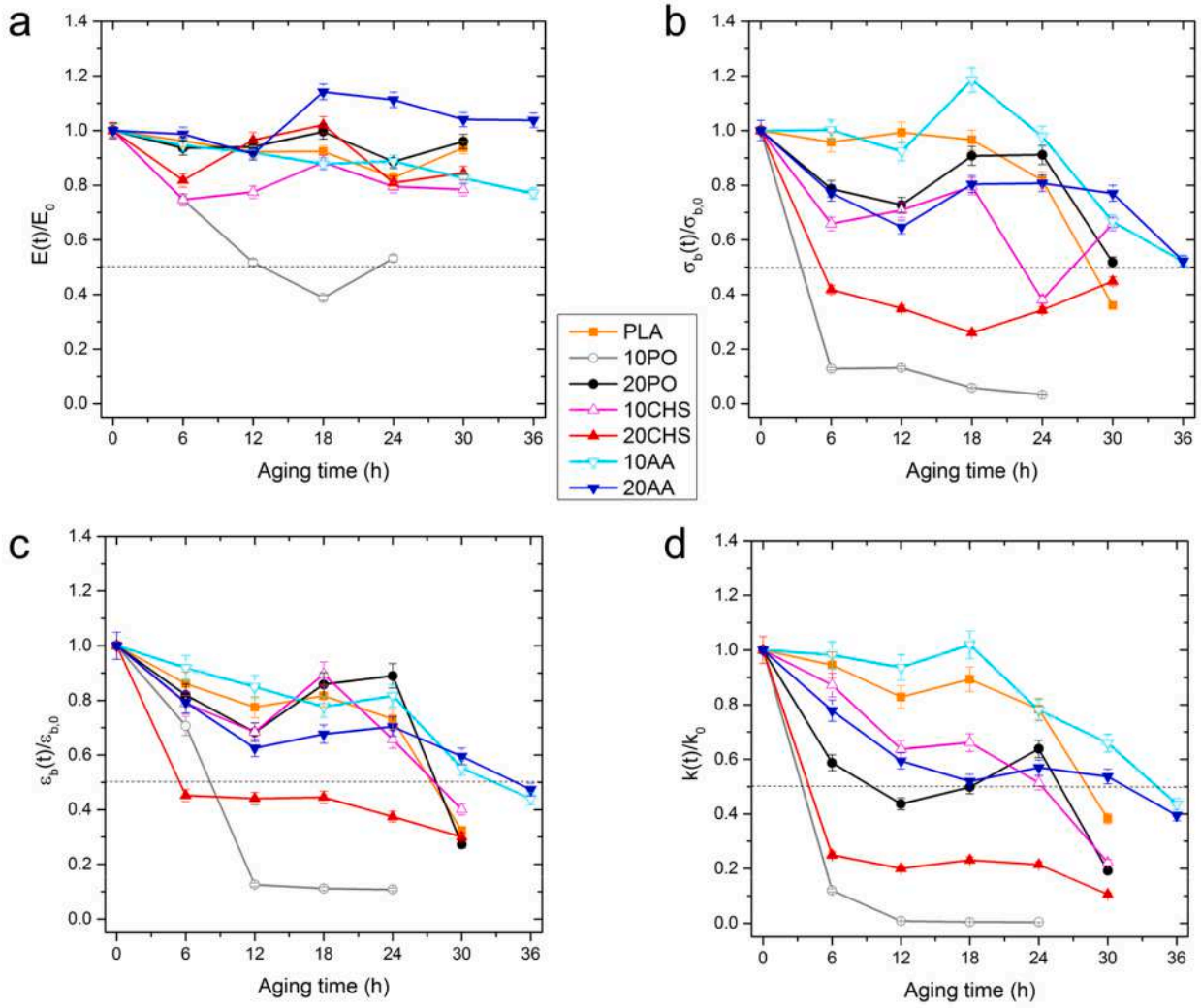

Fig. 5. Evolution of E (a), TS (b), EB (c), and k (d) upon photochemical aging time.

composites is toughness, defined as the work-to-failure (i.e., the area under the stress-strain curve), as it accounts for all the aforementioned mechanical properties.

E initially decreases upon aging but shows a moderate rise after 18–24 h of exposure, likely due to increased crystallization. Most samples retained adequate levels of stiffness, ranging between 80–120% of their initial values, except for 10PO, which showed a significant reduction in E after 18 h and became too brittle to test, breaking into small pieces after 24 h. Neat PLA and other samples containing PO or CH could be tested up to 30 h, while the AA-series composites only showed mechanical degradation after 36 h, indicating enhanced durability.

The analysis of TS and EB reveals a different scenario. Despite some fluctuations, all materials show a decrease in TS over time. This decline is slow for neat PLA and AA-containing composites, moderate for 20PO and 10CH, and exponentially rapid for 10PO and 20CH. The trend of EB over aging time is similar.

Regarding k, which is crucial for practical applications, 10PO and 10CH show a significant loss of mechanical resistance within 6–12 h, while composites with 20% fillers generally experience a halving of toughness between 18 and 24 h. Interestingly, 20AA maintains a constant halved toughness up to 30 h, and neat PLA retains good toughness until 24 h before a sharp decline at 30 h. The highest durability was observed in 10AA.

The overall aging behavior is complex due to the interplay of various phenomena. PLA undergoes progressive weathering, mainly from hydrolytic scission, accelerated by the combined effects of UV irradiation and moisture. These reactions proceed faster in amorphous regions, which are more susceptible to UV and water penetration, and slower in crystalline regions due to the dense packing of macromolecules. Moreover, the crystallinity of the initially amorphous PLA matrix may increase, driven by chain scission or macromolecular rearrangement when stored near T_g [15].

In green composites, the scenario is further complicated. While fillers can promote nucleation, they also increase water uptake, and water diffusion at the filler-matrix interface can significantly contribute to sample degradation. Furthermore, to the best of our knowledge, the combined effects of UV exposure and moisture on lignocellulosic fillers in polymer-based green composites are often insufficiently explored.

Despite differences among the samples, AA demonstrated superior performance, while CH exhibited intermediate, dose-dependent behavior. In contrast, PO acted as a pro-degradant additive; however, composites with 10% PO content performed worse than those containing 20% PO.

During photochemical weathering, the specimens were fixed at the extremities due to the severe tendency of some samples to bend and fold within the UV chamber. PO-series composites showed the strongest

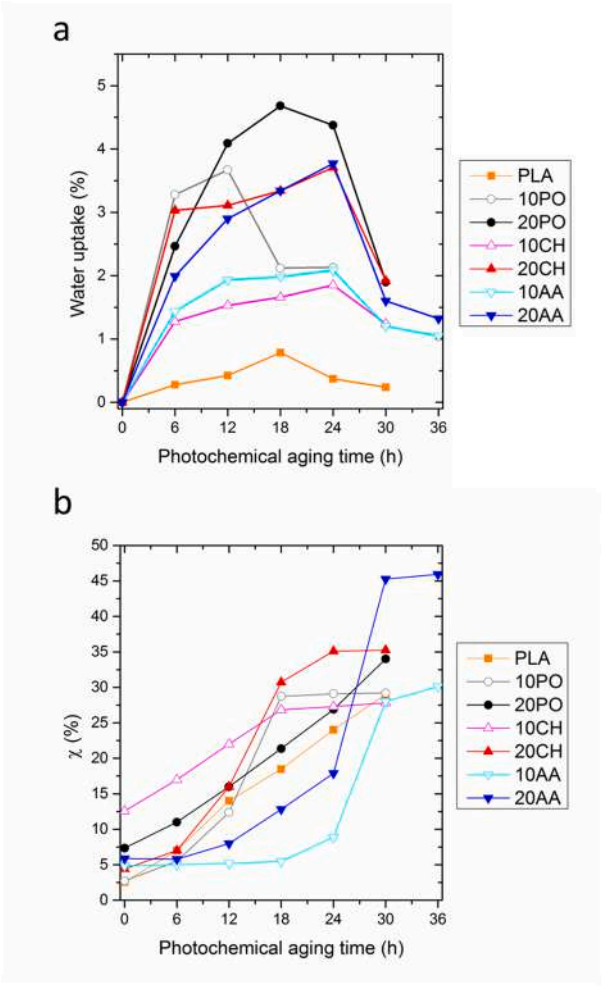

Fig. 6. Evolution of water uptake (a) and crystallinity degree (b) as a function of photochemical aging time.

propensity for self-bending, followed by neat PLA. This behavior was less pronounced in 10CH and 20CH, while it was not observed in the 10AA and 20AA samples.

In summary, the self-folding deformation of PLA and PLA-based green composites during UV irradiation and condensation is primarily driven by differential degradation, thermal gradients, moisture absorption and desorption, internal stresses from fillers, and plasticization and softening of the material induced by UV irradiation and temperatures close to the glass transition, combined with moisture during condensation. These factors collectively cause the specimens to bend or fold within the chamber even in the absence of external stresses.

Fig. 6 provides the evolution over time of water uptake and crystallinity in samples subjected to photochemical aging. Water uptake (Fig. 6a) followed a two-phase behavior: an initial progressive increase in water absorption, followed by a decreasing trend in the latter stage of the experiment (typically after 18 or 24 h). Nonetheless, all final water uptake values exceeded those of unaged samples. Neat PLA, despite reaching a maximum absorption at 18 h, displayed moderate levels of water uptake (below 1%), indicating that water absorption is predominantly influenced by the presence and content of fillers. In this context, the initial porosity of the samples (i.e., the presence of empty lumens and lack of interfacial adhesion) plays a significant role, as does the presence of fillers at the surface, which may offer preferential pathways for water penetration. This is further corroborated by the fact that composites with 20% fillers exhibited water uptake values nearly double those of their 10% filler counterparts, with the only exception being the

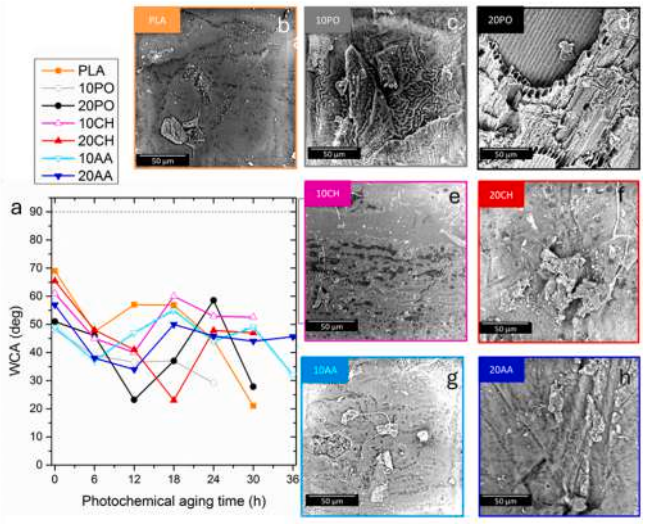

Fig. 7. WCA of the samples as a function of photochemical aging time (a), along with surface SEM micrographs of samples at the end of the experiment (b-h), highlighting the events of surface erosion.

PO-series samples. The most degraded sample, 10PO, showed water uptake similar to that of 20PO, suggesting that the more pronounced deterioration of the matrix is a key factor in water absorption.

After a certain period, all materials exhibited a descending trend in water uptake. In order to elucidate this behavior, DSC tests were performed, and the evolution of crystallinity, calculated using Eq. (4), is shown in Fig. 6b. As expected, all samples demonstrated an increase in crystallinity over time. UV irradiation causes chain scission in the PLA matrix, which promotes crystallization as the shorter chains rearrange into more ordered structures [41]. Lignocellulosic fillers may also act as nucleating agents, enhancing the crystallization of PLA [42]. The degradation process can amplify this effect as the interaction between the degraded PLA chains and the fillers facilitates crystallization, especially when lignocellulosic fillers undergo fragmentation and photodegradation during the experiments. Depending on the formulation, crystallinity evolution can display either linear or sigmoidal patterns, with the onset and final extent of crystallinity varying significantly.

At the end of the experiments, both PLA and composites with 10% filler content achieved a maximum crystallinity of 27–28%, albeit with different kinetics: 10PO and 10CH reached their maximum at 18 h, PLA at 30 h, and 10AA at 36 h, with crystallization triggered in the 5th cycle (24–30 h). For composites containing 20% filler, 20CH and 20PO reached similar final values of approximately 35%, but with distinct trends: 20CH exhibited a sigmoidal increase with a plateau at 24 h, while 20PO showed a linear increase throughout the entire experiment. Meanwhile, 20AA displayed a sigmoidal curve, with a significant increase observed during the fifth cycle (24–30 h), similar to 10AA, but reached a substantially higher final crystallinity (45%).

Notably, all samples showed a crystallinity value of at least 20–25% when the descending trend in water uptake began.

The propagation pathways of photochemical reactions, especially in the presence of condensation cycles and porous fillers, can occur through surface or bulk erosion, or a combination of both. To explore this aspect, the evolution of water contact angle (WCA) over time was investigated and correlated with SEM observations of the exposed surfaces for each sample. Fig. 7 shows the WCA as a function of photochemical aging time for all samples (a), along with SEM micrographs of the surface at the end of the experiment (b-g).

WCA did not follow a monotonic trend. However, consistent with the water uptake results, the final WCA values were always lower than those of the unaged samples. The fluctuations observed in WCA can be

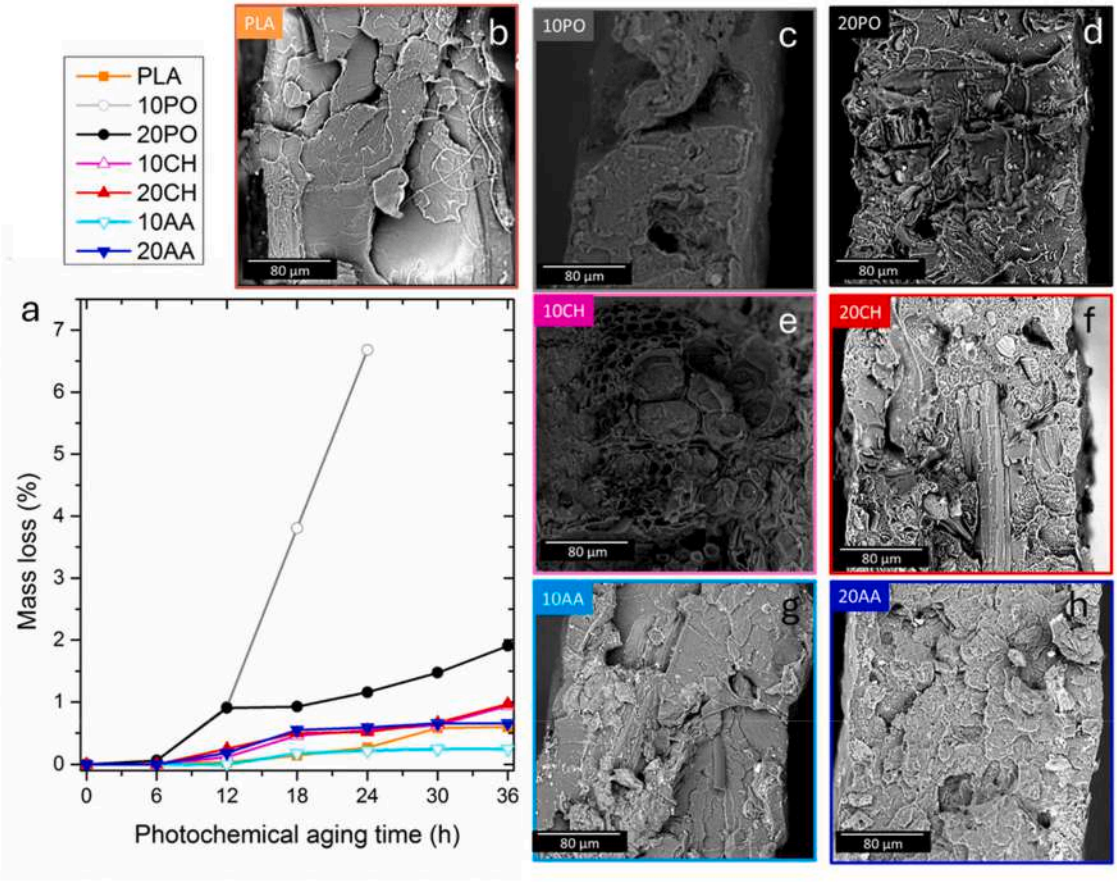

Fig. 8. Mass loss of samples as a function of photochemical aging time, along with cross-sectional micrographs of specimens at the end of the experiment.

reasonably attributed to surface erosion events, as evidenced by SEM micrographs across all samples, particularly those containing PO, where partial or complete ablation of the polymeric layer was observed (Fig. 7c and d). Furthermore, these changes likely result from the interplay of two opposing phenomena:

(i) the exposure of lignocellulosic filler surfaces (which are generally hydrophilic) and the increased surface roughness from chain scission and erosion can decrease the WCA within the initial degradation stages. This can also create more free volume and pathways for water diffusion [43], resulting in higher initial water absorption, in full agreement with the previously discussed water uptake results.

(ii) as the crystalline regions grow and dominate the surface properties, WCA might increase due to the lower surface energy of crystalline PLA [44]. The more ordered and packed structure acts as a barrier to water penetration, leading to a reduction in water uptake over time (see again Fig. 6). However, the presence of lignocellulosic fillers can still contribute to water absorption, although this effect may be diminished by the increased crystallinity of the PLA matrix, which presumably results in a more compact and less etchable surface (as seen in the surface morphology of 45% crystalline 20AA, Fig. 7h).

The fluctuations in WCA over time suggest a continuous and dynamic process of temporary oxidized layer formation and subsequent ablation.

To gain insights into the propagation of degradation phenomena within the bulk, cross-sections of the specimens were analysed, and SEM micrographs of the samples at the end of the experiments, along with the mass loss measurements, are presented in Fig. 8. Mass loss (Fig. 8a) was moderate yet not negligible in most cases, ranging from 0.3% to 1%, except for the PO-based samples, which exhibited mass losses of 1.8% and 7%. It is worth noting that for 10PO, the final mass loss measurement was influenced by the progressive disintegration of the specimens into small pieces within the chamber.

Neat PLA (Fig. 8b) showed internal cracks typical of bulk deterioration, though it lacked significant voids usually associated with bulk erosion, suggesting that surface erosion mechanisms were predominant, consistent with previous results. PO-containing samples (Fig. 8c and d) displayed large cavities with complete fiber-matrix debonding at the interface. Some voids, though less pronounced, were also observed in CH-series composites (Fig. 8e and f), which showed noticeable swelling (see Fig. 8e). In contrast, AA-series samples (Fig. 8g and h) retained their bulk morphology even after long-term exposure.

These results can be explained by considering the initial porosity of the composites and the role of fillers in facilitating water penetration into the core, as well as the quality of interfacial adhesion. PO-based composites, which were already degraded during melt processing, showed the highest water uptake. During condensation cycles, water reacts with the UV-irradiated polymer, and hydrolytic reactions occur both at the surface and within the bulk, especially at the interface. Leaching events may affect not only the polymer matrix but also portions of the fillers. While 20PO exhibited slightly better resistance due to the higher UV-shielding effect of the particles, it still showed a similar degradation mechanism as 10PO, as well as 10CH and 20CH.

According to the scientific literature, mass loss occurs for several reasons, including chain scission events leading to short polymer chains (<20,000 Da), destruction of the filler structure, with formation of soluble compounds, photodegradation products volatilizing as CO_2 [16,40,45–47]. The behavior of AA-series samples was markedly different, with no significant bulk leaching observed through SEM analysis, in agreement with the minimal mass loss measurements. Nonetheless, the

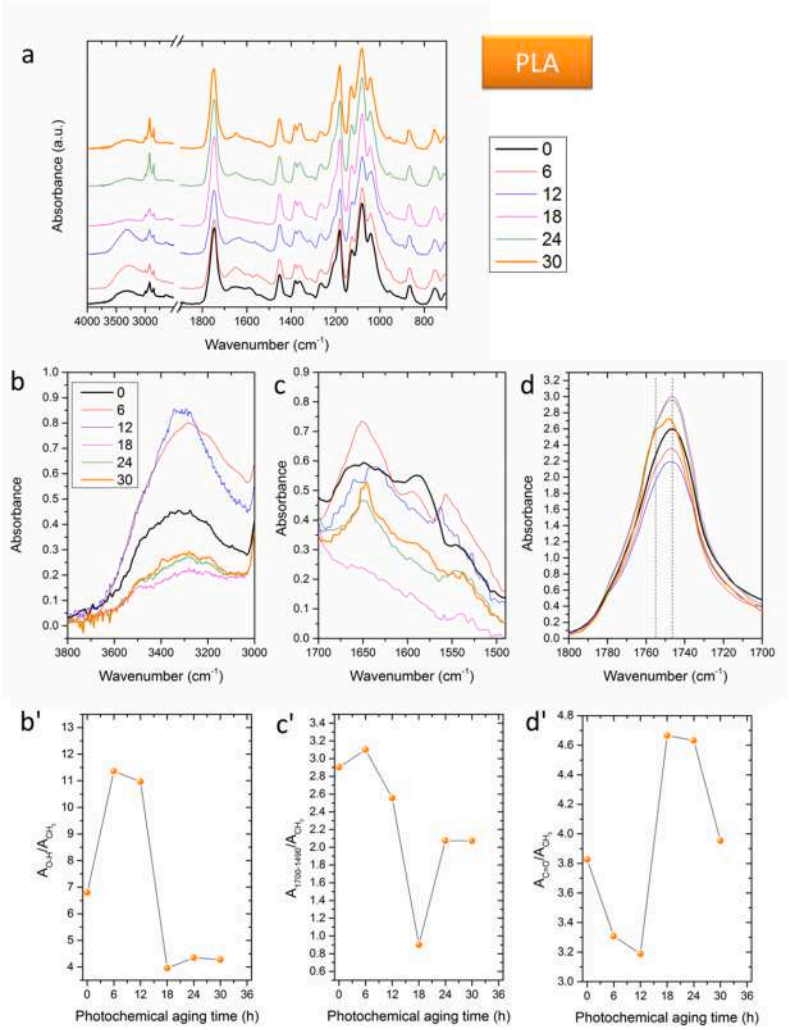

Fig. 9. FTIR/ATR analysis of PLA upon photochemical aging time. Full range spectra normalized to the intensity at 1453 cm^{-1} (a), close-up of the regions: 3800–3000 cm^{-1} (b), 1700–1490 cm^{-1} (c), 1800–1700 cm^{-1} (d), along with the time evolution of the areas under the curve in these three zones, normalized to that of methylene (b'-c'-d').

increase in crystallinity and mechanical decay, although slower and less severe than in other samples, indicate that degradation still occurred. However, it is likely that the molecular weight of the degraded chains did not reach the threshold required for solubilization or volatilization.

To gain deeper insights into the chemical transformations occurring during photochemical aging, FTIR/ATR spectroscopy was performed. The spectra of PLA samples, normalized to the intensity of the CH_3 band at 1452 cm^{-1}, are shown in Fig. 9. For easier readability, Fig. 9b–d display enlarged spectra of three key regions: the 3800–3000 cm^{-1} range, typically attributed to the O—H stretching mode (Fig. 9b); the 1700–1490 cm^{-1} range (Fig. 9c); and the characteristic PLA carbonyl band between 1800–1700 cm^{-1} (Fig. 9d). The quantitative measurements of these variations, calculated as the ratio of each area to that of the methylene group [39], are shown in Fig. 9b'–d'.

In neat PLA, two distinct stages of photochemical aging can be observed. During the initial stage (0–12 h), there is a there is a significant increase in the area under the O—H stretching region (~3020–3700 cm^{-1}), along with the emergence of a complex signal in the 1520–1680 cm^{-1} region.

These changes are generally attributed to the formation of new carbonyl moieties due to α-cleavage of the ester bond in the PLA backbone, as well as the formation of perester, peracid moieties, and double bond functional groups [48]. Additionally, a decrease was observed in both the signal at 1250 cm^{-1} (C—O-C), related to the linkage of repeating units of PLA, and in the carbonyl band, centred at 1747–1478 cm^{-1}.

Taken together, these results suggest an increasing concentration of -COOH and -OH end groups due to hydrolysis, along with the formation of temporary species due to the photochemical aging. Interestingly, after 18 h of exposure, the spectra become more similar to that of the unirradiated sample, indicating the removal of oxidized temporary layers and/or the leaching of hydrosoluble oligomers during condensation. The second stage of aging is marked by the insurgence and progressive growth of a shoulder in the carbonyl band at 1755 cm^{-1}, which suggests increased crystallinity, as clearly shown in Fig. 8d. This observation aligns with the DSC and water uptake behavior previously discussed.

Between 18 and 30 h, the areas under 2500–3300 cm^{-1} (OH region) and 1520–1680 cm^{-1} (representing new carbonyl species and oxidation products) begin to increase again, albeit slowly due to the heightened crystallinity. These findings indicate that the dynamic production and consumption of reactive intermediates continues throughout the process. Interestingly, highly oxidized samples that underwent erosive phenomena exhibit spectra that resemble their unoxidized counterparts. This dynamic evolution is further confirmed by analysing the carbonyl index (Fig. 8c'), which follows an inverse trend to the OH region.

The FTIR/ATR spectra of composites collected at different treatment times are shown in Fig. 10, while the evolution of normalized areas

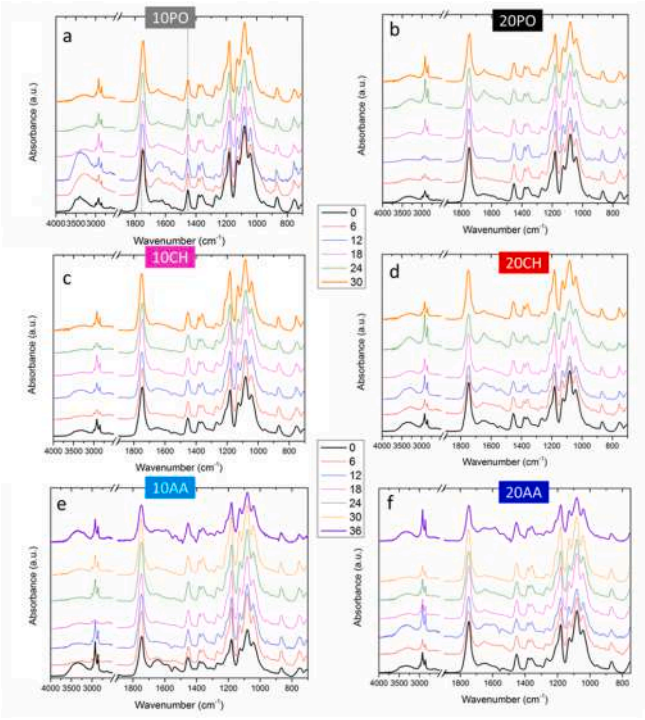

Fig. 10. FTIR/ATR spectra upon photochemical aging time of 10PO (a), 20PO (b), 10CH (c), 20CH (d), 10AA (e), and 20AA (f).

under the OH region (3800–3020 cm^{-1}), the C = O peak (1800–1700 cm^{-1}), and the 1700–1490 cm^{-1} region are presented in Fig. 11a–c for composites with 10% fillers, and in Fig. 11d–f for those with 20% fillers. It can be noted that all green composites exhibit periodic fluctuations in the evolution of the three spectral regions, though with different intervals and amplitudes.

Among the samples, 10PO showed the strongest increase in the areas under both 3800–3020 cm^{-1} and 1700–1490 cm^{-1} during the initial stage of photochemical aging. Thereafter, these areas began to decrease, confirming the leaching/ablation of the most hydrolysed polymer chains and photo-oxidation byproducts. At 30 h, analyses of specimen fragments revealed a renewed rise in these spectral features, indicating the characteristic "zigzag" pattern of erosive mechanisms. 10CH displayed a similar trend, albeit with smaller amplitude variations. In contrast, 10AA exhibited a different pattern, with both the OH region (3800–3020 cm^{-1}) and 1700–1490 cm^{-1} areas showing positive concavity when plotted against aging time, while the C = O index displayed negative concavity. Interestingly, by the end of the experiment, these values matched those of the unirradiated samples, suggesting that 10AA samples also underwent photochemical oxidation, albeit at slower kinetics and to a lesser extent.

For composites with 20% filler loading, the highest content of lignocellulosic fillers may affect the analysis, but the overall zig-zag behavior persisted. In this case, the amplitude of spectral feature variations was more pronounced in 20PO and 20CH, while the spectral features of 20AA remained relatively stable over time. However, even the AA-series samples showed spectra different from their unaged counterparts by the end of the experiments, indicating that photodegradation altered the chemical structure of these samples without causing significant bulk ablation. This finding aligns with SEM observations, as well as the results of water contact angle (WCA), water uptake, and mass loss previously discussed.

Solvent-aided extraction was carried out to gain further insights into the states of both the fillers and the matrix throughout the aging process. Notably, complete separation of the fillers from the matrix became unachievable after prolonged exposure (see Fig. S2). Following extended photo-oxidation, two distinct phases were isolated from each

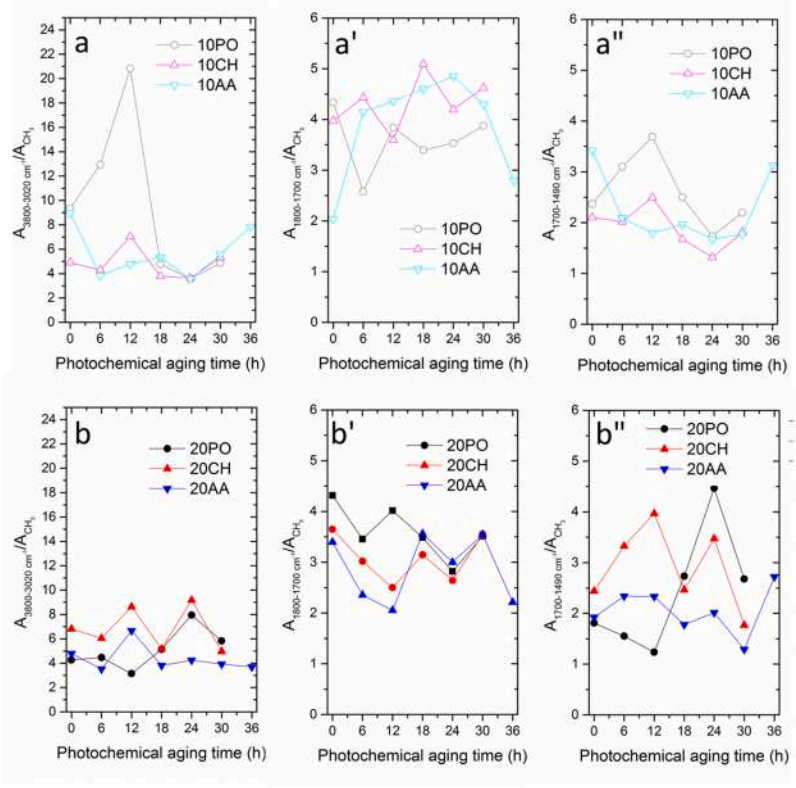

Fig. 11. Evolution of areas under OH region at 3800–3020 cm^{-1} (a-b), C = O region at 1800–1700 cm^{-1} (a'-b') and 1700–1490 cm^{-1} region (a"-b") normalized to those of methylene for composites containing 10% filler (top panels, a-a") and 20% filler (bottom panels, b-b").

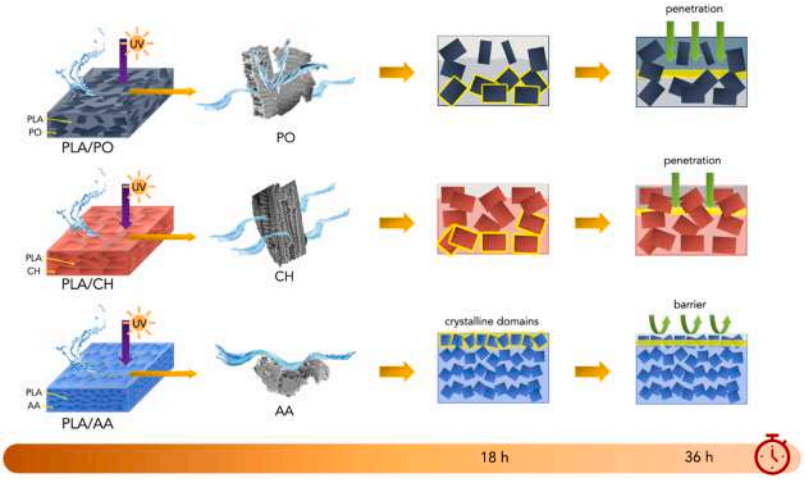

Fig. 12. Pictorial representation of the degradation pathways for the various composite systems. Composites based on PO and CH experience bulk erosion as a result of water penetration, while the more compact AA-based composites are less prone to water absorption. Degradation in AA composites is slower and mostly confined to surface layers. After 18 h, the development of crystalline domains in all systems (see yellow areas) slows degradation kinetics and limits water penetration.

composite: a polymer-enriched phase (Fig. S2a–f) and a filler-enriched phase (Fig. S2a'–f'). In the polymer-enriched phase (Fig. S2a–f), small lignocellulosic fragments were observed floating alongside dissolved polymer, likely due to photochemically induced disruption of lignocellulosic domains. Conversely, the filler-enriched phase (Fig. S2a'–f') showed larger fillers partially surrounded by residual polymeric layers. Analysing these distinct phases provides complementary information on the aging level of both the matrix and fillers.

Interestingly, the 10PO (Fig. 2a) and 10CH (Fig. 2c) samples exhibited the highest amounts of lignocellulosic fragments in the polymer-enriched phase, whereas within the filler-enriched phase, they showed significant polymer residue adhering to larger filler particles (Fig. 2a' and c'), which appeared considerably damaged compared to their unaged counterparts (see Fig. S1). Indeed, the PO (a'-b') and CH (c'-d') fillers extracted from their respective aged composites, displayed cracks and rounded edges. These observations suggest that under this specific weathering protocol, even lignocellulosic fillers underwent degradation. Interestingly, these alterations appeared to enhance filler-matrix interactions, particularly in the most degraded PO and CH samples (panels a-d and a'-d'), and to a lesser extent in 20AA samples, as indicated by the presence of few lignocellulosic fragments trapped in the polymer-enriched phase (Fig. S2f), as well as polymeric residues surrounding the fillers in the filler-enriched phase (Fig. S2f').

Notably, the less-degraded 10AA sample contained the fewest filler fragments in the polymer-enriched phase (Fig. S2e) and exhibited minimal amounts of polymeric layers surrounding the extracted fillers (Fig. S2e'), which closely resembled their unaged counterparts extracted after processing (see Fig. S1).

Fig. 12 provides a schematic illustration of the degradation pathways in the composite systems studied. Highly porous fillers such as PO resulted in less compact composites with lower molar mass, attributed to the pro-degradant activity of the microparticles, and therefore a strong ability to facilitate water penetration into the core. This led to the lowest durability among the tested samples. Hydrolytic scission events propagated rapidly both at the surface and within the bulk, primarily at the matrix-filler interface, resulting in mass loss due to the formation of soluble PLA oligomers and PO constituents. The rapid degradation of 10PO can be attributed to its initially amorphous nature and the reduced UV-shielding effect of the surface particles due to the low filler content.

The CH-series materials exhibited slightly better durability, likely due to the lower porosity of the fibers and the nucleating activity of CH, which, especially at lower concentrations, delayed the degradation pathways. However, the overall degradation mechanism still involved surface erosion and bulk propagation through the matrix-filler interface, similar to PO-based composites.

In contrast, the AA-series materials demonstrated superior durability compared to the other green composites and neat PLA. This can be attributed to the different morphology and chemical composition of AA particles. AA fillers are denser platelets that form more compact composites, and they contain a wide range of antioxidants that can delay the onset of photochemical reactions. Even after 36 h of exposure, although the materials showed signs of chemical alteration, crystallization, and surface erosion, there was no significant leaching observed in the bulk. This aspect indicates that, while degradation was still ongoing, the reaction propagation was considerably slower, thus allowing AA-based composites to retain their integrity for a longer duration. This study highlights that the biodegradable polyesters, prone to hydrolysis under UV and water exposure, may benefit or not from waste biomass fillers depending on specific factors:

(i) filler chemical composition: lignocellulosic fillers can either stabilize the material through UV-shielding and antioxidants or promote degradation via pro-degradant compounds.
(ii) Secondary interactions with the matrix: fillers can limit UV and water penetration if they act as nucleating agents or contribute to a denser morphology with strong interfacial adhesion. Otherwise, they may facilitate bulk degradation.

4. Conclusions

In this work, we assessed the photochemical stability of PLA-based green composites containing three different lignocellulosic fillers, i.e., *Posidonia oceanica* (PO), *Chamaerops humilis* (CH), and *Ailanthus altissima* (AA), all derived from waste biomass but possessing distinct morphology and physicochemical properties. The materials underwent photochemical aging through cycles of UV irradiation followed by condensation and their physicochemical, morphological, and mechanical properties were thoroughly characterized. The results underline the importance of filler selection in tailoring the performance of PLA-based composites for specific applications. Specifically, the pro-degradant activity and high porosity of CH and especially PO fillers led to less compact composites with lower molar mass, accelerating hydrolytic degradation. This caused surface and bulk erosion. Composites with 10% PO showed the lowest stability (less than 6 h), followed by those with 20% CH. Green composites containing 20% PO and 10% CH showed durability of 24–30 h, similar to or slightly lower than neat PLA, owing to the enhanced crystallinity that delayed degradation pathways.

AA-based composites demonstrated the highest durability. The dense

morphology of AA fillers and their antioxidant content delayed photochemical reactions and slowed degradation, allowing these composites to retain their structural integrity even after 36 h of exposure.

Generally, these findings demonstrate that durability of composites can be designed by tailoring the filler chemical composition, such as the content of antioxidants or pro-degradant compounds, and by other interactions between filler and matrix, including nucleating effect, porosity, interfacial adhesion, which impact UV and water propagation into the bulk.

Furthermore, by repurposing waste biomass, this study demonstrates the dual benefit of mitigating the environmental impact of local invasive species while advancing the development of durable and sustainable composite materials for outdoor applications.

CRediT authorship contribution statement

Andrea Maio: Writing – review & editing, Writing – original draft, Visualization, Validation, Supervision, Software, Methodology, Investigation, Funding acquisition, Formal analysis, Data curation, Conceptualization. **Emmanuel F. Gulino:** Visualization, Software, Investigation, Funding acquisition, Formal analysis, Data curation. **Michele Gammino:** Software, Investigation, Data curation. **Maria Clara Citarrella:** Visualization, Software, Investigation. **Roberto Scaffaro:** Writing – review & editing, Supervision, Resources, Project administration, Methodology, Funding acquisition, Conceptualization.

Declaration of competing interest

The authors declare that they have no known competing financial interests or personal relationships that could have appeared to influence the work reported in this paper.

Acknowledgements

We are grateful for financial support of MICS (Made in Italy – Circular and Sustainable) Extended Partnership and received funding from the European Union Next-GenerationEU (PIANO NAZIONALE DI RIPRESA E RESILIENZA (PNRR) – MISSIONE 4 COMPONENTE 2, INVESTIMENTO 1.3 – D.D. 1551.11-10-2022, PE00000004), for financial support of SiciliAn MicronanOTecH Research And Innovation CEnter "SAMOTHRACE" (MUR, PNRR-M4C2, ECS_00000022), spoke 3 - Università degli Studi di Palermo "S2-COMMs - Micro and Nanotechnologies for Smart & Sustainable Communities, and for financial support of "New recyclable thermosetting and elastomeric polymeric materials based on bio-renewable feedstocks Extended Partnership" (PRIN: PROGETTI DI RICERCA DI RILEVANTE INTERESSE NAZIONALE – Bando 2022 PIANO NAZIONALE DI RIPRESA E RESILIENZA (PNRR) Prot. P2022K9XN3 CUP: B53D23025750001. Authors gratefully acknowledge the financial support provided by the Italian Ministry of Education, University and Research (MIUR) under the PRIN2022 - P20228WNZ2Z. "Green composites based on biodegradable polymers and vegetal biomasses of Mediterranean area: processing, characterization and degradability" CUP: 20228WNZ2Z_001.

We are also grateful to Professor Antonino Valenza and his research group for kindly allowing us to use their DSC equipment.

Supplementary materials

Supplementary material associated with this article can be found, in the online version, at doi:10.1016/j.polymdegradstab.2025.111204.

Data availability

Data will be made available on request.

References

[1] S. Al-Malaika, P. Dubois, P. Gijsman, H. Zahalka, Polymers, environment and sustainable developments: opportunities and recommendations for the coming decade, Polym. Degrad. Stab. 143 (2017) 104–105, https://doi.org/10.1016/j.polymdegradstab.2017.06.021.

[2] F.P. La Mantia, M. Morreale, Green composites: a brief review, Compos. Part A Appl. Sci. Manuf. 42 (2011) 579–588, https://doi.org/10.1016/j.compositesa.2011.01.017.

[3] A. Maio, R. Scaffaro, Multifunctional green composites based on plasma-activated and GO-coated dwarf palm fibers, Compos. Part A Appl. Sci. Manuf. 180 (2024) 108096, https://doi.org/10.1016/j.compositesa.2024.108096.

[4] R. Scaffaro, F. Lopresti, L. Botta, A. Maio, Mechanical behavior of Polylactic acid/Polycaprolactone porous layered functional composites, Compos. Part B Eng. 98 (2016) 70–77, https://doi.org/10.1016/j.compositesb.2016.05.023.

[5] R. Scaffaro, A. Maio, Integrated ternary bionanocomposites with superior mechanical performance via the synergistic role of graphene and plasma treated carbon nanotubes, Compos. Part B Eng. 168 (2019), https://doi.org/10.1016/j.compositesb.2019.03.076.

[6] R. Scaffaro, A. Maio, F. Sutera, E.F. Gulino, M. Morreale, Degradation and recycling of films based on biodegradable polymers: a short review, Polym. (Basel) 11 (2019), https://doi.org/10.3390/polym11040651.

[7] R. Scaffaro, A. Maio, M. Gammino, F.P. La Mantia, Effect of an organoclay on the photochemical transformations of a PBAT/PLA blend and morpho-chemical features of crosslinked networks, Polym. Degrad. Stab. 187 (2021) 109549, https://doi.org/10.1016/j.polymdegradstab.2021.109549.

[8] R. Scaffaro, M.C. Citarrella, Stable and reusable electrospun bio-composite fibrous membranes based on PLA and natural fillers for air filtration applications, Sustain. Mater. Technol. 42 (2024) e01146, https://doi.org/10.1016/j.susmat.2024.e01146.

[9] R. Scaffaro, E.F. Gulino, M.C. Citarrella, Multifunctional 3D-printed composites based on biopolymeric matrices and tomato plant (Solanum lycopersicum) waste for contextual fertilizer release and Cu(II) ions removal, Adv. Compos. Hybrid Mater. 7 (2024) 95, https://doi.org/10.1007/s42114-024-00908-4.

[10] M.C. Mistretta, F.P. La Mantia, V. Titone, L. Botta, M. Pedeferri, M. Morreale, Effect of ultraviolet and moisture action on biodegradable polymers and their blend, J. Appl. Biomater. Funct. Mater. 18 (2020) 1–8, https://doi.org/10.1177/2280800020926653.

[11] M.H. Tran, D.-P. Phan, E.Y. Lee, Review on lignin modifications toward natural UV protection ingredient for lignin-based sunscreens, Green Chem. 23 (2021) 4633–4646, https://doi.org/10.1039/D1GC01139A.

[12] H. Sadeghifar, A. Ragauskas, Lignin as a UV light blocker—a review, Polym. (Basel) 12 (2020), https://doi.org/10.3390/polym12051134.

[13] M. Gammino, C. Gioia, A. Maio, R. Scaffaro, G. Lo Re, Chemical-free Reactive Melt Processing of Biosourced Poly(butylene-succinate-adipate) for Improved Mechanical Properties and Recyclability, ACS Appl. Polym. Mater. 6 (2024) 5866–5877, https://doi.org/10.1021/acsapm.4c00514.

[14] R. Scaffaro, A. Maio, E.F. Gulino, Hydrolytic degradation of PLA/Posidonia Oceanica green composites: a simple model based on starting morpho-chemical properties, Compos. Sci. Technol. 213 (2021) 108930, https://doi.org/10.1016/j.compscitech.2021.108930.

[15] M. Baiamonte, M. Rapisarda, M.C. Mistretta, G. Impallomeni, F.P. La Mantia, P. Rizzarelli, Wood flour and hazelnut shells polylactide-based biocomposites for packaging applications: characterization, photo-oxidation, and compost burial degradation, Polym. Compos. (2024), https://doi.org/10.1002/pc.28439.

[16] W. Wang, G. Ye, D. Fan, Y. Lu, P. Shi, X. Wang, B. Bateer, Photo-oxidative resistance and adjustable degradation of poly-lactic acid (PLA) obtained by biomass addition and interfacial construction, Polym. Degrad. Stab. 194 (2021) 109762, https://doi.org/10.1016/j.polymdegradstab.2021.109762.

[17] R. Scaffaro, A. Maio, M. Gammino, Hybrid biocomposites based on polylactic acid and natural fillers from Chamaerops humilis dwarf palm and Posidonia oceanica leaves, Adv. Compos. Hybrid Mater. 5 (2022) 1988–2001, https://doi.org/10.1007/s42114-022-00534-y.

[18] L. Wu, J. Ding, In vitro degradation of three-dimensional porous poly(D,L-lactide-co- glycolide) scaffolds for tissue engineering, Biomaterials 25 (2004) 5821–5830, https://doi.org/10.1016/j.biomaterials.2004.01.038.

[19] L. Lu, S.J. Peter, M.D. Lyman, H.-L. Lai, S.M. Leite, J.A. Tamada, J.P. Vacanti, R. Langer, A.G. Mikos, In vitro degradation of porous poly(l-lactic acid) foams, Biomaterials 21 (2000) 1595–1605, https://doi.org/10.1016/S0142-9612(00)00048-X.

[20] M.A. Elsawy, K.-H. Kim, J.-W. Park, A. Deep, Hydrolytic degradation of polylactic acid (PLA) and its composites, Renew. Sustain. Energy Rev. 79 (2017) 1346–1352, https://doi.org/10.1016/j.rser.2017.05.143.

[21] T. Zhang, S. Zhou, X. Gao, Z. Yang, L. Sun, D. Zhang, A multi-scale method for modeling degradation of bioresorbable polyesters, Acta Biomater. 50 (2017) 462–475, https://doi.org/10.1016/j.actbio.2016.12.046.

[22] A. Gleadall, J. Pan, M.-A. Kruft, M. Kellomäki, Degradation mechanisms of bioresorbable polyesters. Part 1. Effects of random scission, end scission and autocatalysis, Acta Biomater. 10 (2014) 2223–2232, https://doi.org/10.1016/j.actbio.2013.12.039.

[23] Y. Ratna Kumari, K. Ramanaiah, A.V. Ratna Prasad, K. Hemachandra Reddy, S. Prasad Sanaka, A. Kalyan Prudhvi, Experimental investigation of water absorption behaviour of sisal fiber reinforced polyester and sisal fiber reinforced poly lactic acid composites, Mater. Today Proc. (2021), https://doi.org/10.1016/j.matpr.2020.11.002.

[24] R. Scaffaro, A. Maio, E.F. Gulino, G. Pitarresi, Lignocellulosic fillers and graphene nanoplatelets as hybrid reinforcement for polylactic acid: effect on mechanical properties and degradability, Compos. Sci. Technol. 190 (2020), https://doi.org/10.1016/j.compscitech.2020.108008.
[25] R. Scaffaro, A. Maio, E.F. Gulino, B. Megna, Structure-property relationship of PLA-Opuntia Ficus Indica biocomposites, Compos. Part B Eng. 167 (2019), https://doi.org/10.1016/j.compositesb.2018.12.025.
[26] R. Scaffaro, A. Maio, E.F. Gulino, G. Alaimo, M. Morreale, Green composites based on PLA and agricultural or marine waste prepared by FDM, Polym. (Basel) 13 (2021), https://doi.org/10.3390/polym13091361.
[27] J. Qian, J. Gao, Z. He, S. Yi, Self-shrinking Ailanthus altissima substrate obtained by ultrasonic-assisted treatment: density and pore structure characteristics, Ind. Crops Prod. 175 (2022) 114221, https://doi.org/10.1016/j.indcrop.2021.114221.
[28] R. Scaffaro, A. Maio, F. Lopresti, Physical properties of green composites based on poly-lactic acid or Mater-Bi® filled with Posidonia Oceanica leaves, Compos. Part A Appl. Sci. Manuf. 112 (2018) 315–327, https://doi.org/10.1016/j.compositesa.2018.06.024.
[29] S. Tanasković, S. Gvozdenac, R. Kolarov, V. Bursić, B. Konstantinović, D. Prvulović, Antifeeding and insecticidal activity of Ailanthus altissima and Morus alba extracts against gipsy moth (Lymantria dispar (L.), lepidoptera, lymantridae) larvae under laboratory conditions, J. Entomol. Res. Soc. 23 (2021) 197–212, https://doi.org/10.51963/jers.v23i3.1989.
[30] Y.-N. Mo, F. Cheng, Z. Yang, X.-F. Shang, J.-P. Liang, R.-F. Shang, B.-C. Hao, X.-H. Wang, H.-J. Zhang, A. Wali, C.-F. Lu, Y. Liu, Antioxidant activity and the potential mechanism of the fruit from ailanthus altissima swingle, Front. Vet. Sci. 8 (2021), https://doi.org/10.3389/fvets.2021.784898.
[31] H.R. Mohamed, E.A. El-Wakil, E.-S.S. Abdel-Hameed, M.M. El-Hashash, M. Shemis, Evaluation of total phenolics, flavonoids, and antioxidant and cytotoxic potential of ailanthus altissima (Mill.) swingle leaves, J. Reports Pharm. Sci. 10 (2021) 130–136, https://doi.org/10.4103/jrptps.JRPTPS_7_21.
[32] H.R. Mohamed, E.A. El-Wakil, M.M. El-Hashash, E.-S.S. Abdel-Hameed, Chemical constituents of Ailanthus altissima (Mill.) swingle leaves growing in Egypt and their antioxidant activity, Acta Pharm. Sci. 61 (2023) 213–233, https://doi.org/10.23893/1307-2080.APS6115.
[33] S.B. Song, G.J. Chung, H.J. Jung, J.Y. Jang, H.Y. Chung, N.D. Kim, J.-H. Lee, K. Min, S.Y. Park, C.S. Kwak, E.S. Hwang, Suppression of reactive oxygen species generation as a part of antioxidative effect of plant extracts, Korea. J. Food Sci. Technol. 53 (2021) 706–714, https://doi.org/10.9721/KJFST.2021.53.6.706.
[34] Y. Du, T. Wu, N. Yan, M.T. Kortschot, R. Farnood, Fabrication and characterization of fully biodegradable natural fiber-reinforced poly(lactic acid) composites, Compos. Part B Eng. 56 (2014) 717–723, https://doi.org/10.1016/j.compositesb.2013.09.012.
[35] O.F. Solomon, I.Z. Ciută, Détermination de la viscosité intrinsèque de solutions de polymères par une simple détermination de la viscosité, J. Appl. Polym. Sci. 6 (1962) 683–686, https://doi.org/10.1002/app.1962.070062414.
[36] J.R. Dorgan, J. Janzen, D.M. Knauss, S.B. Hait, B.R. Limoges, M.H. Hutchinson, Fundamental solution and single-chain properties of polylactides, J. Polym. Sci. Part B Polym. Phys. 43 (2005) 3100–3111, https://doi.org/10.1002/polb.20577.
[37] R. Scaffaro, M. Gammino, A. Maio, Wet electrospinning-aided self-assembly of multifunctional GO-CNT@PCL core-shell nanocomposites with spider leg bioinspired hierarchical architectures, Compos. Sci. Technol. 221 (2022) 109363, https://doi.org/10.1016/j.compscitech.2022.109363.
[38] R. Scaffaro, A. Maio, M. Gammino, G. Alaimo, Modelling the structure-property relationships of high performance PBAT-based biocomposites with natural fibers obtained from Chamaerops humilis dwarf palm, Compos. Sci. Technol. 223 (2022) 109427, https://doi.org/10.1016/j.compscitech.2022.109427.
[39] M.E. González-López, A.S. Martín del Campo, J.R. Robledo-Ortíz, M. Arellano, A. A. Pérez-Fonseca, Accelerated weathering of poly(lactic acid) and its biocomposites: a review, Polym. Degrad. Stab. 179 (2020) 109290, https://doi.org/10.1016/j.polymdegradstab.2020.109290.
[40] D. Rasselet, A. Ruellan, A. Guinault, G. Miquelard-Garnier, C. Sollogoub, B. Fayolle, Oxidative degradation of polylactide (PLA) and its effects on physical and mechanical properties, Eur. Polym. J. 50 (2014) 109–116, https://doi.org/10.1016/j.eurpolymj.2013.10.011.
[41] X. Liu, X. Hua, H. Wu, Degradation behavior of poly (lactic acid) during accelerated photo-oxidation: insights into structural evolution and mechanical properties, J. Polym. Environ. 32 (2024) 3810–3821, https://doi.org/10.1007/s10924-024-03211-x.
[42] H. Simmons, P. Tiwary, J.E. Colwell, M. Kontopoulou, Improvements in the crystallinity and mechanical properties of PLA by nucleation and annealing, Polym. Degrad. Stab. 166 (2019) 248–257, https://doi.org/10.1016/j.polymdegradstab.2019.06.001.
[43] G. Xian, Y. Niu, X. Qi, J. Tian, C. Li, Q. Yue, R. Guo, Water absorption and property evolution of epoxy resin under hygrothermal environment, J. Mater. Res. Technol. 31 (2024) 3982–3997, https://doi.org/10.1016/j.jmrt.2024.07.123.
[44] T. Paragkumar N, D. Edith, J.-L. Six, Surface characteristics of PLA and PLGA films, Appl. Surf. Sci. 253 (2006) 2758–2764, https://doi.org/10.1016/j.apsusc.2006.05.047.
[45] N. Lesaffre, S. Bellayer, H. Vezin, G. Fontaine, M. Jimenez, S. Bourbigot, Recent advances on the ageing of flame retarded PLA: effect of UV-light and/or relative humidity, Polym. Degrad. Stab. 139 (2017) 143–164, https://doi.org/10.1016/j.polymdegradstab.2017.04.007.
[46] M. Gardette, S. Thérias, J.-L. Gardette, M. Murariu, P. Dubois, Photooxidation of polylactide/calcium sulphate composites, Polym. Degrad. Stab. 96 (2011) 616–623, https://doi.org/10.1016/j.polymdegradstab.2010.12.023.
[47] Y. Yu, Y. Yao, T.M. Adyel, S. Shahid Iqbal, J. Wu, L. Miao, J. Hou, Characterization of the dynamic aging and leached dissolved organic carbon from biodegradable and conventional plastics under photooxidation, J. Environ. Manage. 349 (2024) 119561, https://doi.org/10.1016/j.jenvman.2023.119561.
[48] P. Bhati, A. Srivastava, R. Ahuja, P. Chauhan, P. Vashisth, N. Bhatnagar, Physicochemical Properties of UV-Irradiated, Biaxially Oriented PLA Tubular Scaffolds, Polymers (Basel). 15 (2023), https://doi.org/10.3390/polym15051097.